Published in final edited form as:
Inorganica Chim Acta. 2012 March 15; 382: 19–26. doi:10.1016/j.ica.2011.09.056.

Preparation of aluminum(III) (bis(amido)pyridine)(thiolate) complexes: unexpected transmetalation mediated by $LiAlH_4$

Yosra M. Badiei, **Yunbo Jiang**, **Leland R. Widger**, **Maxime A. Siegler**, and **David P. Goldberg**
Department of Chemistry, Johns Hopkins University, Baltimore, Maryland, 21218, USA

Abstract

Treatment of an unsymmetrical bis(imino)pyridyl-thiolate zinc(II) complex [$Zn^{II}(LN_3S)(OTf)$] (**1**) with $LiAlH_4$ results in the double reduction of the two imino groups in the ligand backbone, and at the same time causes a rare transmetalation reaction to occur. The products formed in this reaction are two novel aluminium(III) bis(amido)pyridyl-thiolate complexes [(*R,S/S,R*-[$Al^{III}(LH_2N_3S)$(THF)] (**2a**) and [(*R,R/S,S*-[$Al^{III}(LH_2N_3S)$(THF)] (**2b**), which are diastereomers of each other. These complexes have been characterized by single-crystal X-ray diffraction and ^{1}H NMR spectroscopy. Single crystal X-ray structure analysis shows that the Al^{III} ion is bound in an almost idealized square pyramidal geometry in **2a**, while being held in a more distorted square pyramidal geometry in **2b**. The major difference between **2a** and **2b** arises in the orientation of the terminal methyl groups of the ligand backbone in relation to the $Al^{III}N_3S$ plane. These two complexes are crystallized at different temperatures (room temperature vs −35 °C), allowing for their separate isolation. Structural analysis shows that these complexes are reduced by the formal addition of one hydride ion to each imino group, resulting in a deprotonated bis(amido)pyridyl-thiolate ligand. A detailed analysis of metrical parameters rules out the possibility of pure one- or two-electron reduction of the π-conjugated bis(imino)pyridine framework. ^{1}H NMR spectra reveal a rich pattern in solution indicating that the solution state structures for **2a** and **2b** match those observed in the solid-state crystal structures, and reveal that both complexes are severely conformationally restricted. Direct organic synthetic methods failed to produce the reduced bis(amino)pyridyl-thiol ligand in pure form, but during the course of these efforts an unusual unsymmetrical aminopyridyl ketone, 1-(6-(1-(2,6-diisopropylphenylamino)ethyl)pyridin-2-yl)ethanone was synthesized in good yield and can be used as a possible precursor for further ligand development.

Keywords

aluminum; bis(imino)pyridine; transmetalation; zinc; ligand reduction; ligand design

1. Introduction

The tridentate 2,6-bis(imino)pyridine (2,6-BIP) platform has played an important role in a broad range of reactions, including olefin polymerizations, Fe- and Co-centered dinitrogen reduction, and alkane oxidation catalysis [1, 2]. It also exhibits rich redox behavior,

Correspondence to: David P. Goldberg.

Appendix A. Supplementary material
Supplementary data associated with this article can be found, in the online version, at doi:xxx.

providing a site for storing reducing equivalents in conjunction with redox-active metals (e.g. Fe, Ni) [3–10]. Given the usefulness and versatility of this ligand, significant synthetic efforts have gone into modifying the steric and electronic properties of the BIP-type framework, either by substitution of the typical aryl imino substituents, or other methods [11—17]. A particular challenge arises when confronted with preparing desymmetrized analogs of the parent BIP ligand 2,6-$(ArN=CMe)_2(C_5H_3N)$ in which the Ar substituents are different. These unsymmetrical derivatives are desirable for applications from catalysis [18–20] to synthetic bioinorganic analogs of enzyme active sites [21]. With regard to the latter goal, we are interested in developing mixed N,S donor ligands for preparing models of non-heme iron enzymes such as superoxide reductase and cysteine dioxygenase (CDO) [22–27]. Ligand design to target these centers is non-trivial because of the difficulties posed in making unsymmetrical N,S-systems. We recently employed the BIP platform to successfully prepare the unsymmetrical complex $[Fe^{II}(LN_3S)(OTf)]$ via a metal-assisted template reaction, which served as a structural and functional model of the $His_3Cys\text{-}Fe^{II}$ center found in substrate-bound CDO [26].

To modify, and possibly enhance, the reactivity of our nonheme iron models with O_2, we sought a more electron-rich version of the LN_3S ligand, and therefore targeted the synthesis of the reduced, bis(amino)pyridine analog. Although bis(amino)pyridine systems have been sought for their use in catalysis, relatively few such compounds have been prepared [14, 28, 29]. For example, the synthesis of 2,6-bis(2,6-diisopropylphenylaminomethyl)pyridine was accomplished by addition of LiNHAr (Ar = 2,6-di-isopropylphenyl) to 2,6-bis(bromomethyl)pyridine [28]. However, this double alkylation strategy is not practical for the synthesis of unsymmetrical derivatives.

Herein we report the successful reduction of the bis(imino) functionalities in the unsymmetrical LN_3S ligand, starting from the zinc(II) complex $[Zn(LN_3S)(OTf)]$ (**1**). During this work a rare transmetalation reaction was discovered, leading to the isolation and structural characterization of the neutral Al^{III} complexes $[Al(LH_2N_3S)(THF)]$ (**2a–b**). This facile transmetalation process has potential implications for the role of Al cocatalysts in olefin polymerizations with BIP ligands.

2. Experimental

2.1 General Procedures

All reactions were carried out under an atmosphere of N_2 or Ar using a drybox or standard Schlenk techniques unless noted otherwise. All reagents were purchased from commercial vendors and used without further purification unless noted otherwise. Diethyl ether and dichloromethane were purified via a Pure-Solv Solvent Purification System from Innovative Technology, Inc. All solvents were degassed by repeated cycles of freeze-pump-thaw and then stored in an N_2-filled drybox. Methanol was distilled over CaH_2. The pyridyliminoketone, 2-(O=CMe)-6-(2,6-iPr_2-C_6H_3N=CMe)-C_5H_3N was synthesized according to the literature [18]. The zinc complex $Zn^{II}(LN_3S)(OTf)$ (**1**) was synthesized as described previously [26].

2.2 Physical Methods

NMR was performed on a Bruker Avance 400 MHz FT-NMR spectrometer at 25 °C. Elemental analysis was performed by Atlantic Microlab Inc., Norcross, GA. LDI-ToF mass spectra were obtained using a Bruker Autoflex III Maldi ToF/ToF instrument (Billerica, MA). Samples were dissolved in Et_2O or CH_2Cl_2 and deposited on the target plate in the absence of any added matrix. Samples were irradiated with a 355 nm UV laser and mass - analyzed by ToF mass spectrometry in the reflectron mode.

2.3 Synthesis of R,S/S,R-[Al^{III}(LH_2N_3S)(THF)]•1/2Et_2O (2a•1/2Et_2O)

To a chilled slurry of Zn(LN_3S)OTf (430 mg, 0.670 mmol) in 15 mL THF at −35 °C (the solution was pre-cooled in the drybox freezer (−35 °C) for 10 min) was added 0.60 mL of $LiAlH_4$ solution (1 M) dropwise. Bubbling was observed and the solution turned from red to a green-yellow color with the formation of a yellow precipitate as the reaction warmed to room temperature. The solution was stirred for 2 h at r.t., and then the THF was concentrated in vacuo to ca. 1 mL. Diethyl ether (10 mL) was added, and the solution was filtered on a fine frit. The filtrate was concentrated in vacuo, and slow evaporation over 1 d yielded **2a** as yellow crystals (30 %). ^{1}H NMR (CD_2Cl_2) δ 8.02 (t, 1H, J = 7.7 Hz, Py-H_p), 7.53 (d, 1H, J = 7.7 Hz, Py-H_m), 7.45 (d, 1H, J = 7.7 Hz, Py-H_m), 7.14-7.05 (m, 4H, Ar-H), 6.83 (t, 1H, J = 7.6 Hz, Ar-H), 6.43 (d, 1H, J = 7.3 Hz, Ar-H), 6.30 (t, 1H, J = 7.3 Hz, Ar-H), 4.82 (q, 1H, J = 6.4 Hz, CHPy), 4.30 (q, 1H, J = 6.8 Hz, CHPy), 4.00 (br, 2H, CH_2 (THF), 3.77 (m, 3H, CH_2(THF), one set of $CHMe_2$ resonances is buried under this THF peak), 2.82 (m, 1H, J = 6.8 Hz, $CHMe_2$), 1.89 (br, 4 H, CH_2(THF)), 1.55 (d, 3H, J = 6.4 Hz, Me-CHPy), 1.40 (d, 3H, J = 6.8 Hz, Me-CHPy), 1.26 (d, 3H, J = 6.8 $CHMe_2$), 1.25 (d, 3H, J = 6.8 $CHMe_2$), 1.09 (d, 3H, J = 6.8 $CHMe_2$), 1.02 (d, 3H, J = 6.8 $CHMe_2$). Diethyl ether (0.5 equiv.) is found in the ^{1}H NMR spectrum (δ 3.45, 1.15) and is in agreement with the Et_2O found in the crystal lattice by X-ray structural analysis. The crystal structure of **2a** also suggests that there should be minor contamination from the other racemic pair (*S,S/R,R*) of diastereomers. However, NMR analysis of bulk crystalline material does not reveal peaks that correspond to this isomer (**2b**), indicating it is not present in any significant quantity. ^{13}C NMR (CD_2Cl_2) δ 163.0, 162.5, 149.5, 148.5, 148.4, 140.4, 130.5, 129.4, 124.4, 123.9, 122.9, 122.8, 119.4, 119.1, 113.4, 107.3, 65.8, 28.1, 27.4, 25.8, 25.5, 25.1, 24.0, 21.1, 20.3, 15.2. LDIMS(+): m/z 458 [**2a** – THF + H]$^+$. Anal. Calcd. for $C_{33}H_{45}AlN_3O_{1.5}S$ (**2a**•1/2($C_4H_{10}O$)), C, 69.93; H, 8.00; N, 7.41. Found C, 69.38; H, 7.45; N, 8.79.

2.4 Synthesis of R,R/S,S-[Al^{III}(LH_2N_3S)(THF)] (2b)

The mother liquor from crystallizations of **2a** was separated and layered with pentane (Et_2O to pentane ratio 8:1), and left to stand at −35 °C for 2 d, affording X-ray quality crystals of diastereoisomer **2b**. ^{1}H NMR (CD_2Cl_2) δ 7.51 (t, 1H, J = 7.2 Hz, Py-H_p), 7.39 (d, 1H, J = 7.6 Hz, Py-H_m), 7.16 (d, 1H, J = 7.6 Hz, Py-H_m), 7.09 (t, 1H, J = 6.4 Hz Ar-H), 7.04-6.96 (m, 3H, Ar-H), 6.88 (d, 1H, J = 8.0 Hz, Ar-H), 6.58 (t, 2H, J = 7.6 Hz, Ar-H), 4.72 (br, 1H, CHPy), 4.20 (br, 1H, CHPy), 3.92 (br, 2H, CH_2 (THF), 3.68 (br, 2H, CH_2 (THF)), 3.23 (m, 2H, J = 6.8 Hz, $CHMe_2$), 1.82 (br, 4 H, CH_2(THF)), 1.61 (d, 3H, J = 6.4 Hz, Me-CHPy), 1.46 (d, 3H, J = 6.4 Hz, Me-CHPy), 1.22 (d, 6H, J = 6.8 Hz, $CHMe_2$), 1.02 (d, 6H, J = 6.8 Hz, $CHMe_2$).

2.5 Synthesis of 1-(6-(1-(2,6-diisopropylphenylamino)ethyl)pyridin-2-yl)ethanone (3)

Under ambient conditions, 1-(6-(1-(2,6-diisopropylphenylimino)ethyl)pyridin-2-yl)ethanone (1.0 g, 3.10 mmol) was dissolved in a 1:1 mixture of $CHCl_3$/MeOH before $NaBH_4$ (117 mg, 3.10 mmol) was added in small portions. The reaction was monitored by TLC, and after 2 h the reaction had reached completion. The reaction mixture was concentrated in vacuo, and the crude oil was re-dissolved in $CHCl_3$, washed twice with water, dried and concentrated. Purification by column chromatography on silica (EtOAc/hexanes) gave **3** as pure yellow solid. Yield 561 mg (56%). ^{1}H NMR ($CDCl_3$) δ 8.29 (d, 1H), 7.81 (t, 1H), 7.36 (d, 1H), 7.17 (d, 2H), 7.10 (t, 1H), 4.96 (m, 1H), 4.57 (d, 1H), 2.74 (m, 2H), 2.23 (s, 3H), 1.57 (d, 3H), 1.15 (d, 12H); ^{13}C NMR ($CDCl_3$) δ 166.7, 162.1, 154.9, 146.6, 137.7, 136.0, 123.9, 123.3, 121.2, 120.0, 68.8, 28.6, 24.5, 23.5, 23.2, 17.6.

2.6 X-ray structure determinations

All reflection intensities were measured at 110(2) K using a KM4/Xcalibur (detector: Sapphire3) with enhanced graphite-monochromated Mo Kα radiation (λ = 0.71073 Å) under the program CrysAlisPro (Version 1.171.33.55, Oxford Diffraction Ltd., 2010). The program CrysAlisPro (Version 1.171.33.55, Oxford Diffraction Ltd., 2010) was used to refine the cell dimensions. Data reduction was done using the program CrysAlisPro (Version 1.171.33.55, Oxford Diffraction Ltd., 2010). The structure was solved with the program SHELXS-97 (Sheldrick, 2008) and was refined on F2 with SHELXL-97 (Sheldrick, 2008) [30]. Analytical numeric absorption corrections based on a multifaceted crystal model were applied using CrysAlisPro (Version 1.171.33.55, Oxford Diffraction Ltd., 2010). The temperature of the data collection was controlled using the system Cryojet (manufactured by Oxford Instruments). The H-atoms were placed at calculated positions (except for that located on C14) using the instructions AFIX 13, AFIX 23, AFIX 43 or AFIX 137 with isotropic displacement parameters having values 1.2 or 1.5 times Ueq of the attached C atoms. The position and the isotropic temperature factor of the H atom located on C14 (i.e., H14) were refined freely. The distance C14−H14 was restrained to be 1.00(1) Å. Relevant crystallographic data and structure refinement parameters for these complexes are summarized in Table 1.

2.6.1 Complex 2a—The structure of the compound $C_{31}H_{40}AlN_3OS{\cdot}½(C_4H_{10}O)$ **2a** was solved and refined in the centrosymmetric space group *P* $\bar{1}$ with *Z'* = 1. The asymmetric unit contains one molecule of the Al complex and one lattice diethyl ether solvent molecule (with an occupancy factor of 0.5). The lattice solvent molecule is found disordered over a center of inversion (½, ½, 0). The atom C8/C8' (methyl group located on C7) is disordered over two positions such that the chirality on C7 is either *R* or *S*. The major component of the disorder (C8) refines to an occupancy of 0.819(6). There is no evidence that suggests disorder for atom C15 (methyl group located on C14). Disorder on C15 may not occur because of steric effects from the isopropyl group C22/C23/C24. The C7 and C14 atoms have opposite chirality (*i.e.*, C7RC14S or C7SC14R) approximately 82% of the time, and have the same chirality (*i.e.*, C7RC14R or C7SC14S) approximately the rest of the time.

2.6.2 Complex 2b—The structure of the compound $C_{31}H_{40}AlN_3OS$ was solved and refined in the centrosymmetric space group *P* $\bar{1}$ with *Z'* = 2. The asymmetric unit contains two crystallographically independent molecules of the Al complex. The diastereoisomers that are found in the crystal lattice are *S,S* and *R,R*. Some residual electron density was found in one large void volume located approximately at (½, 0, 1), which includes 65 electrons in a volume of 346 $Å^3$. The void likely contains unresolved solvent molecules. The contribution of the unresolved residual electron density was then taken out for the subsequent stages of the refinement using the program SQUEEZE [31].

3. Results and discussion

3.1 Synthesis

The key desymmetrization for the BIP platform occurs with the synthesis of the pyridyliminoketone, 2-(O=CMe)-6-(2,6-iPr_2-C_6H_3N=CMe)-C_5H_3N (Scheme 1), previously reported by Bianchini and coworkers [18]. This precursor bears a single 2,6-diisopropylphenyl substituent, which provides steric protection of the subsequently derived thiolate-ligated complexes. An obvious strategy to obtain the bis(amino) derivative involves reductive amination of the imino-ketone with 2-aminothiophenol, but this reaction failed to give the desired product under a variety of conditions. Simple condensation to give the mixed imine was also problematic; the standard methods for Schiff base formation proved unsuccessful, giving only mixtures of unidentified products or recovered starting materials

(Scheme 1). A third route involved initial reduction of the pyridyliminoketone to the pyridylaminoketone 2-(O=CMe)-6-(2,6-iPr_2-C_6H_3NHCHMe)-C_5H_3N **3**, which proceeded smoothly with $NaBH_4$ (Scheme 2). However, attempts to form the imine with 2-aminothiophenol and **3** also either failed to react, or gave only unwieldy mixtures of products. Compound **3** also proved to be an ineffective substrate for the metal-assisted template reaction used in the synthesis of **1**. It is likely that the difficulties encountered in condensation of **3** with 2-aminothiophenol is a result of the presence of the nucleophilic thiol group. The 2-aminothiophenol is known to be problematic when condensing with ketones because both the N and S groups may add to the carbonyl carbon atom to give a thiazoline [32]. Thus compound **3** should be useful as a key precursor to forming other types of unsymmetrical, polydentate pyridine-based ligands.

We next investigated the reduction of the zinc complex (**1**) as an alternative strategy for synthesizing a reduced bis(amino) derivative (Scheme 3). Complex **1** was prepared via a zinc template reaction, as previously described [26]. Treatment of **1** with $LiAlH_4$ at −35 °C in THF for 1 h led to a color change from red to yellow-green with the formation of a yellow precipitate. The solution was warmed and stirred for an additional 2 h at room temperature. After work-up and recrystallization from Et_2O/THF, yellow crystals (blocks) suitable for crystal structure determination were obtained. The X-ray structure revealed that a surprising transmetalation reaction had occurred, and the Zn^{II} ion was replaced by an Al^{III} ion bound in the tetradentate N_3S(thiolate) site, giving complex **2a**. The molecular structure for **2a** is shown in Figure 1. A THF molecule occupies the fifth coordination site at the Al^{III} center, while a noncoordinating molecule of Et_2O is found in the lattice in the ratio 2 (**2a**) : 1 Et_2O. The absence of any counterions in the crystal lattice indicates that the ligand must carry a 3^- charge to balance the trivalent Al ion.

The trianionic charge of the tetradentate ligand may arise from the reduction of the two imine bonds by addition of two hydride ions, which would lead to the former imino N donors being converted to two monoanionic amido donors. An alternate configuration would result from the addition of two electrons to the conjugated π system of the bis(imino)pyridine framework. The reduction of the conjugated π framework in aryl-substituted bis(imino)pyridine metal complexes by one or two electrons to give monoanionic or dianionic (monoradical or diradical) ligands has been observed for a number of metal complexes, including Al^{III} bis(imino)pyridine complexes [8]. In general this ligand “non-innocence” is of interest because of fundamental questions related to electronic structure, as well as for the potential implications regarding redox-based reactivity of the ligand-metal complex. Both $1e^-$- and $2e^-$-reductions have occurred when [Fe(^{i}PrPDI)$(Cl)_2$] (^{i}PrPDI = 2,6-(2,6-$^i Pr_2C_6H_3N$=CMe)$_2C_5H_3N$) was treated with the hydride donor $NaBEt_3H$, giving mono- or diradical products [33, 34]. Thus the possibility of electron-transfer to the ligand in **1** following treatment with $LiAlH_4$ was carefully considered (*vide infra*).

3.2 Structural analysis

Relevant bond lengths and angles for **2a** are summarized in Table 2, together with data for related complexes. The angles about C(7) and C(14) in **2a** range between 105.9 – 115.8°, suggesting sp^3 hybridization, as opposed to the angles between 113.7° – 115.7° found in the zinc(II) starting material **1**, which contains sp^2-hybridized imino carbon atoms. In addition, the methyl groups in **2a** (C(8) and C(15)) do not lie in the same plane as the pyridine and former C_{imine}-N groups, as would be expected for mono- or di-radical ligand structures [8, 34]. The C_{imine}-N_{imine} distances in **1** are 1.278(3) and 1.283(3) Å. These distances are significantly elongated in **2a**, C(7)–N(1) = 1.462(3) Å and C(14)–N(3) = 1.465(3) Å, whereas the C(7/14)-C_{ipso} bonds in **2a** are nearly identical to those in **1** (1.517(4), 1.520(4) Å for 4compared to 1.501(4), 1.497(4) Å in **1**). In contrast, pure $1e^-$- or $2e^-$-reduction of the bis(imino)pyridine framework is expected to result in only a modest elongation of the

C_{imine}-N_{imine} bonds; density functional theory (DFT) calculations for a hypothetical bis(imino)pyridine zinc(II) complex reveal 0.03 – 0.05 Å elongation of the C_{imine}-N_{imine} bonds upon $1e^-$ or $2e^-$ reduction [34]. Similarly, modest contractions of the C_{imine}-C_{ipso} single bonds (0.04 – 0.06 Å) are calculated for the reduced Zn^{II} structures. The same trends are observed for the crystallographically characterized $1e^-$- and $2e^-$-reduced Fe complexes [Fe(^{i}PrPDI)(Cl)], [Fe(^{i}PrPDI)(N_2)$_2$] and [Fe(^{i}PrPDI)(DMAP)] [34]. Finally, the H atom on C(14) was located in the difference map of the X-ray structure for **2a**, supporting the assignment of C(14) as an sp^3-hybridized tertiary carbon center. All of the metrical parameters for the bis(imino)pyridine backbone in **2a** are consistent with hydride addition to the imino bonds in **1**, and show no evidence for $1e^-$- or $2e^-$-reduction in the conjugated π system.

The former analysis strongly indicates that the N_3S donor in **2a** is best described as a fully deprotonated, bis(amido)pyridylthiolate ligand. The short Al–N distances of Al–N(1) = 1.887(2) Å and Al–N(3) = 1.862(2) Å for **2a** are in good agreement with other bis(amido) donors. For example, a mixed pyridyl(imino)(amido) aluminum(III) compound derived from treatment of the parent 2,6-bis(imino)pyridine ligand with $AlMe_3$ reported by Bruce and coworkers [35] exhibits a short, deprotonated N_{amido}–Al distance = 1.876(4) Å. These Al^{III}-N bonds are significantly shorter than the Zn^{II}-N (2.202(2); 2.173(2) Å) and Fe^{II}-N (2.188(2); 2.184(2) Å) bond lengths observed in **1** and [Fe^{II}(LN_3S)(OTf)], respectively [27], or the Al^{III}-N(H)RR' bond lengths of 2.090(5) and 2.098(5) Å seen in the complex [((*R*,*R*)-R_4-salcyan)Al(OH)] [36], where the amine donor is protonated. Furthermore, the Al^{III}-S distance in **2a** (2.2798(9) Å) falls in the reported range for other Al^{III}-SR bond lengths (2.220(1) to 2.5226(6) Å) [37–39].

The geometry of the Al^{III} ion is nearly an idealized square pyramid (sp) based on its τ value, which is a quantitative angular parameter that distinguishes between purely square pyramidal and trigonal bipyramidal (tbp) geometries in 5-coordinate complexes. For **2a**, τ = 0.01, where (sp) $0 \leq \tau \leq 1$ (tbp)) [40]. The Al atom lies 0.402(3) Å above the basal plane defined by the N_3S donor set toward the axially ligated THF molecule. In comparison, the Zn^{II} ion for **1** exhibits a more distorted square pyramidal geometry with τ = 0.09, and sits further away (0.471(4) Å) from the N_3S plane. The analogous Fe^{II} complex [Fe^{II}(LN_3S)(OTf)] is also distorted square pyramidal (τ = 0.12) with an even larger Fe-to-plane distance of 0.540(3) Å.

From the former structural data we conclude that complex **1** has been fully reduced by $LiAlH_4$ to give two deprotonated, anionic amido donors, and the Zn^{II} ion has been replaced by Al^{III} via a novel transmetalation reaction. The fate of the Zn^{II} ion in this process is not known, although we speculate that it is likely released into solution as zinc triflate/hydride salts, that may in part form insoluble byproducts. A white precipitate forms following treatment of **1** with $LiAlH_4$ and warming up of the reaction mixture, and this material may contain some of the displaced Zn^{II} ion as an insoluble byproduct.

3.3 Mechanistic considerations

The facile reduction of imine bonds by strong hydride donors such as $LiAlH_4$ is well known. It is therefore reasonable to conclude that the reaction of **1** with $LiAlH_4$ occurs through hydride addition to the imine bonds in **1** in a first step, which is then followed by transmetallation of Zn^{II} by Al^{III}. Evidence for this mechanism was obtained from laser desorption ionization mass spectrometry (LDI-MS). Analysis of the white solid that is produced during the reaction was performed by LDI-MS, and revealed a prominent isotopic cluster centered at *m/z* = 496.14 (Figure S1). The isotope pattern matches that for $[Zn^{II}LH_4N_3S]^+$ (theor. *m/z* = 496.18), and can be assigned to the fully reduced Zn^{II} complex, in which both imine bonds have been reduced and the resulting N donors are

protonated (from isolation in air). A small peak is also observed at *m/z* = 494.13, which can be assigned to the Zn^{II} product in which only one of the imine bonds has been reduced ($[Zn^{II}(LH_2N_3S)]^+$, theor. *m/z* = 494.16). These data indicate that the reduction of the imine bonds of the zinc(II) starting material most likely occurs prior to the transmetallation process.

To provide further evidence for the proposed mechanistic sequence, we examined the reaction of **1** with a different hydride source, $NaBH_4$, which does not contain the Al^{III} ion. Addition of 1.5 equiv of $NaBH_4$ to **1** in MeOH/EtOH at r.t. led to the formation of a yellow solid as seen for $LiAlH_4$. This solid was filtered and isolated by aerobic work-up and analyzed by LDI-MS. A prominent isotopic cluster at *m/z* = 494.00 was observed, corresponding to the singly reduced Zn^{II} complex $[Zn^{II}(LH_2N_3S)]^+$ (Figure S2). Although this procedure is not useful for obtaining the fully reduced product, it provides clear evidence that imine reduction readily occurs directly for the Zn^{II} complex, and does not require Al^{III}. This result supports our overall proposed mechanism in which reduction of the imine bonds in **1** is relatively facile, and occurs prior to Al^{III} transmetalation.

3.4 Stereochemistry

The structural data for the Al^{III} complex **2a** are consistent with one diastereomeric pair (*R,S/S,R*) being formed in the reduction reaction. However, reduction of **1** with $LiAlH_4$ is not expected to proceed with diastereoselectivity, and we wondered whether the other *R,R/S,S* diastereomeric pair was formed in this reaction. Recrystallization of the mother liquor that was separated from **2a** by layering with pentane at −35 °C afforded a new batch of yellow crystalline blocks (Scheme 2). Structural analysis of these new crystals revealed that they were not a second crop of **2a**, but a new complex **2b** (Figure 2). Relevant bond lengths and angles are summarized in Table 2 for one of the two independent molecules in the unit cell (both molecules exhibit similar bond distances and angles, and therefore only one set of bond distances and angles are given as representative of the structure). As seen in **2a**, the tetradentate LH_2N_3S ligand forms the basal plane around a transmetalated Al^{III} ion, with a molecule of THF occupying the axial position. The key difference seen for **2b** as compared to **2a** lies in the orientation of the methyl groups attached to the former imino carbon atoms (C(7a) and C(14a)). In **2b**, these methyl groups can be seen as oriented *anti* in relation to the AlN_3 plane, whereas for **2a** these groups are positioned s*yn* across this plane. Reduction of both imine bonds of **2b** is confirmed by the former C_{imine}-N_{imine} and C_{imine}-C_{ipso} distances, as well as the non-planarity of C(7a) and C(14a). The Al–N distances of Al–N(1) = 1.8763(13) Å and Al–N(3) = 1.8560(13) Å for **2b** are in good agreement with the deprotonated N_{amido}–Al distance. It is worth noting that the geometry of complex **2b** is distorted with τ values of 0.31 and 0.24 corresponding to the two independent molecules in the unit cell. In addition, the Al ion is 0.338(2) Å or 0.354(2) Å above the basal plane for the two independent molecules. Thus complex **2b** is the second diastereomeric pair (*R,R/S,S*) produced in the reduction/transmetalation reaction, and shows that there is no strong diastereomeric preference for this reaction. The different orientation of the methyl groups does not cause any significant changes in bond lengths, but subtle changes are induced about the Al ^{III} coordination sphere such that the geometry is now significantly distorted from idealized square pyramidal, as seen for **2a**.

3.5 ^{1}H NMR spectra

As seen in the solid-state X-ray structure, reduction of the imine bonds in **1** produces two chiral centers at the ketimine carbon atoms, and the structure of **2a** consists of the racemate of the *S,R/R,S* diastereomer [41]. The ^{1}H NMR spectrum of **2a** in CD_2Cl_2 is shown in Figure 3. The two new C-H resonances resulting from the reduction of the imino carbon atoms are significantly separated and can be found as quartets at δ 4.82 (*J* = 6.4 Hz) and 4.30 (*J* = 6.8

Hz) ppm. The adjacent methyl groups are also distinct, and shifted upfield as expected from 2.79 and 2.43 ppm in **1** to 1.55 (J = 6.4 Hz) and 1.40 (J = 6.8 Hz) ppm in **2a**. The isopropyl methine resonances are even further separated by ~1 ppm, appearing at 3.77 (overlapped with THF) and 2.82 ppm (septet). This latter ~1 ppm separation clearly indicates that rotation is highly restricted about the C(ipso)-N bond of the diisopropylphenyl substituent. Interestingly, all four ^{i}Pr-Me groups also give rise to distinct resonances. One pair of doublets appears at 1.09 and 1.01 ppm, while the other pair appears as overlapping doublets at 1.26 ppm. The former data indicate that the rotational freedom about the ^{i}Pr groups is hindered, pointing to the highly crowded nature of the complex. The solution state structure for **2a** matches the solid state, and reveals that the complex is severely conformationally restricted.

Although the limited solubility of **2b** in CD_2Cl_2 leads to a less well-resolved ^{1}H NMR spectrum (Figure 4), comparisons can still be made between the solution state structures of **2a** and **2b**, revealing significant differences for the two complexes. The resonances for the new backbone C-H protons in **2b** (δ 4.72 and 4.20 ppm) are each shifted upfield by 0.1 ppm in comparison to **2a**, while the adjacent methyl groups are shifted slightly downfield for **2b** to δ 1.61 and 1.46 ppm. Interestingly, large changes in the resonances for the ^{i}Pr groups for **2b** versus **2a** are seen. The ^{i}Pr-CH methine groups in **2b** are no longer separated as in **2a**, but appear as a broad, overlapping mutliplet at 3.23 ppm. In addition, all four ^{i}Pr-CH_3 doublets are separated for **2a**, but for **2b** the ^{i}Pr-CH_3 resonances can be assigned to two doublets centered at 1.22 and 1.02 ppm. The NMR data for **2b** are consistent with hindered rotation about the diisopropylphenyl C(ipso)-N bond as seen for **2a**, but the fact that the ^{i}Pr-CH and ^{i}Pr-CH_3 peaks are not well-separated in **2b** are consistent with the different solid-state structures of **2b** versus **2a**. The ^{i}Pr-C(25) in **2a** is likely more crowded than the corresponding C(25A) in **2b** because of the positioning of the methyl group C(15), which lies on the same side of the chelate ring as the THF molecule, in proximity to C(25). From the ^{1}H NMR analysis, it is clear that both **2a** and **2b** maintain their solid state structures in solution.

4. Concluding remarks

The synthesis and characterization of two new thiolate-containing Al(III) bis(amido)pyridylthiolate complexes was accomplished via reduction of a Zn^{II} bis(imino)pyridylthiolate precursor complex with $LiAlH_4$. The synthesis of the reduced bis(amino)pyridylthiol ligand could not be accomplished by conventional organic synthetic strategies, and thus the success with the zinc(II) complex **1** as starting material highlights the usefulness of metal template chemistry in the preparation of unsymmetrical frameworks such as **1**. Interestingly, during the reduction process a rare transmetallation reaction occurs, producing the Al^{III} products.

The BIP systems have been extensively studied as supporting ligands for Fe- and Co-catalyzed olefin oligomerizations and polymerizations, and aluminum-containing cocatalysts (methylaluminoxane (MAO), AlR_3) are essential for these reactions. Significant efforts have been made to discern the role of the aluminum co-catalysts, but this role remains poorly understood. Evidence has been presented by other workers to indicate that transmetalation with Al may be an important factor in the activity of these catalytic systems [8, 35, 42]. Of particular relevance here is the work from Gambarotta and co-workers, which showed that BIP-Fe^{II} complexes react with AlR_3 in an unexpected transmetalation process to give Al^{III} products [8]. In this reaction the BIP ligand was reduced by electrons delocalized on to the π-system, resulting in paramagnetic Al complexes. The ability of BIP ligands to exist in such “non-innocent” reduced states [5, 10] suggests the possibility of a non-innocent configuration for **2a–b**, and thus such a configuration was carefully considered. However,

the structural parameters and diamagnetic ^{1}H NMR spectra for **2a–b** clearly rule out this possibility. The transformation of **1** to **2a–b** is only the second example of an Al-mediated transmetalation reaction with the BIP system besides that reported by Gambarotta [8], and is the only case in which the BIP framework remains “innocent”. Taken together, these results suggest that aluminum transmetalation may be a more general phenomenon than was apparent from the original report by Gambarotta, and could be of potential importance in the mechanism of olefin polymerizations catalyzed by the widely used Al -dependent (BIP)M^{II} systems.

Supplementary Material

Refer to Web version on PubMed Central for supplementary material.

Acknowledgments

The financial support from the National Institutes of Health (GM62309) to D.P.G. is gratefully acknowledged. Y. J. is grateful for an Ernest M. Marks Fellowship.

References

1. Gibson VC, Redshaw C, Solan GA. Chem. Rev. 2007; 107:1745–1776. [PubMed: 17488059]
2. Knijnenburg Q, Gambarotta S, Budzelaar PHM. Dalton Trans. 2006:5442–5448. [PubMed: 17117213]
3. Bowman AC, Bart SC, Heinemann FW, Meyer K, Chirik PJ. Inorg. Chem. 2009; 48:5587–5589. [PubMed: 19361163]
4. Manuel TD, Rohde JU. J. Am. Chem. Soc. 2009; 131:15582–15583. [PubMed: 19860475]
5. Wieder NL, Gallagher M, Carroll PJ, Berry DH. J. Am. Chem. Soc. 2010; 132:4107–4109. [PubMed: 20199024]
6. Russell SK, Darmon JM, Lobkovsky E, Chirik PJ. Inorg. Chem. 2010; 49:2782–2792. [PubMed: 20143847]
7. Scott J, Vidyaratne I, Korobkov I, Gambarotta S, Budzelaar PHM. Inorg. Chem. 2008; 47:896–911. [PubMed: 18173261]
8. Scott J, Gambarotta S, Korobkov I, Knijnenburg Q, de Bruin B, Budzelaar PHM. J. Am. Chem. Soc. 2005; 127:17204–17206. [PubMed: 16332066]
9. Enright D, Gambarotta S, Yap GPA, Budzelaar PHM. Angew. Chem., Int. Ed. 2002; 41:3873–3876.
10. Gallagher M, Wieder NL, Dioumaev VK, Carroll PJ, Berry DH. Organometallics. 2010; 29:591–603.
11. Griffith GA, Al-Khatib MJ, Patel K, Singh K, Solan GA. Dalton Trans. 2009:185–196. [PubMed: 19081988]
12. Steves JE, Kennedy MD, Chiang KP, Kassel WS, Dougherty WG, Dudley TJ, Zubris DL. Dalton Trans. 2009:1214–1222. [PubMed: 19322494]
13. Ionkin AS, Marshall WJ, Adelman DJ, Fones BB, Fish BM, Schiffhauer MF. Organometallics. 2006; 25:2978–2992.
14. Britovsek GJP, England J, Spitzmesser SK, White AJP, Williams DJ. Dalton Trans. 2005:945–955. [PubMed: 15726149]
15. Lappalainen K, Yliheikkila K, Abu-Surrah AS, Polamo M, Leskela M, Repo T, Anorg Z. Allg. Chem. 2005; 631:763–768.
16. Zhang TZ, Sun WH, Li T, Yang XZ. J. Mol. Catal. A-Chem. 2004; 218:119–124.
17. Davis RN, Tanski JM, Adrian JC, Tyler LA. Inorg. Chim. Acta. 2007; 360:3061–3068.
18. Bianchini C, Mantovani G, Meli A, Migliacci F, Zanobini F, Laschi F, Sommazzi A. Eur. J. Inorg. Chem. 2003:1620–1631.
19. Ionkin AS, Marshall WJ, Adelman DJ, Fones BB, Fish BM, Schiffhauer MF, Soper PD, Waterland RL, Spence RE, Xie TY. J. Polym. Sci., Part A: Polym. Chem. 2008; 46:585–611.

20. Xie GY, Li TC, Zhang AQ. Inorg. Chem. Commun. 2010; 13:1199–1202.
21. Kendall AJ, Zakharov LN, Gilbertson JD. Inorg. Chem. 2010; 49:8656–8658. [PubMed: 20799715]
22. Krishnamurthy D, Kasper GD, Namuswe F, Kerber WD, Sarjeant AAN, Moënne-Loccoz P, Goldberg DP. J. Am. Chem. Soc. 2006; 128:14222–14223. [PubMed: 17076472]
23. Namuswe F, Kasper GD, Sarjeant AAN, Hayashi T, Krest CM, Green MT, Moënne-Loccoz P, Goldberg DP. J. Am. Chem. Soc. 2008; 130:14189–14200. [PubMed: 18837497]
24. Namuswe F, Hayashi T, Jiang YB, Kasper GD, Sarjeant AAN, Moenne-Loccoz P, Goldberg DP. J. Am. Chem. Soc. 2010; 132:157–167. [PubMed: 20000711]
25. Stasser J, Namuswe F, Kasper GD, Jiang YB, Krest CM, Green MT, Penner-Hahn J, Goldberg DP. Inorg. Chem. 2010; 49:9178–9190. [PubMed: 20839847]
26. Jiang YB, Widger LR, Kasper GD, Siegler MA, Goldberg DP. J. Am. Chem. Soc. 2010; 132:12214–12215. [PubMed: 20712312]
27. Badiei YM, Siegler MA, Goldberg DP. J. Am. Chem. Soc. 2011; 133:1274–1277. [PubMed: 21207980]
28. Britovsek GJP, Gibson VC, Mastroianni S, Oakes DCH, Redshaw C, Solan GA, White AJP, Williams DJ. Eur. J. Inorg. Chem. 2001:431–437.
29. Jie S, Diaconescu PL. Organometallics. 2010; 29:1222–1230.
30. Sheldrick GM. Acta Crystallogr. A. 2008; 64:112–122. [PubMed: 18156677]
31. Spek AL. Acta Crystallogr. D. 2009; 65:148–155. [PubMed: 19171970]
32. Fahmi N, Singh RV. Transit. Metal Chem. 1994; 19:453–456.
33. Bouwkamp MW, Bart SC, Hawrelak EJ, Trovitch RJ, Lobkovsky E, Chirik PJ. Chem. Commun. 2005:3406–3408.
34. Bart SC, Chlopek K, Bill E, Bouwkamp MW, Lobkovsky E, Neese F, Wieghardt K, Chirik PJ. J. Am. Chem. Soc. 2006; 128:13901–13912. [PubMed: 17044718]
35. Bruce M, Gibson VC, Redshaw C, Solan GA, White AJP, Williams DJ. Chem. Commun. 1998:2523–2524.
36. Nixon TD, Dalgarno S, Ward CV, Jiang ML, Halcrow MA, Kilner C, Thornton-Pett M, Kee TP, Chimie CR. 2004; 7:809–821.
37. Lien YL, Chang YC, Chuang NT, Datta A, Chen SJ, Hu CH, Huang WY, Lin CH, Huang JH. Inorg. Chem. 2010; 49:136–143. [PubMed: 19950963]
38. Chen IC, Ho SM, Chen YC, Lin CY, Hu CH, Tu CY, Datta A, Huang JH, Lin CH. Dalton Trans. 2009:8631–8643. [PubMed: 19809740]
39. Reddy ND, Kumar SS, Roesky HW, Vidovic D, Magull J, Noltemeyer M, Schmidt HG. Eur. J. Inorg. Chem. 2003:442–448.
40. Addison AW, Rao TN, Reedjik J, van Rijn J, Verschoor GC. Dalton Trans. 1984:1349–1456.
41. Some minor positional disorder of C(8) is observed for **2a**, and modeling of this disorder leads to an estimate of the population of the two diastereomers of 82% for the *S,R/R,S* pair, and 18% for the *S,S/R,R* pair. However, ^{1}H NMR data show no evidence of the *S,S/R,R* isomer in the bulk solid, suggesting the population of the minor component is much less than 18%.
42. Knijnenburg Q, Smits JMM, Budzelaar PHM. Organometallics. 2006; 25:1036–1046.

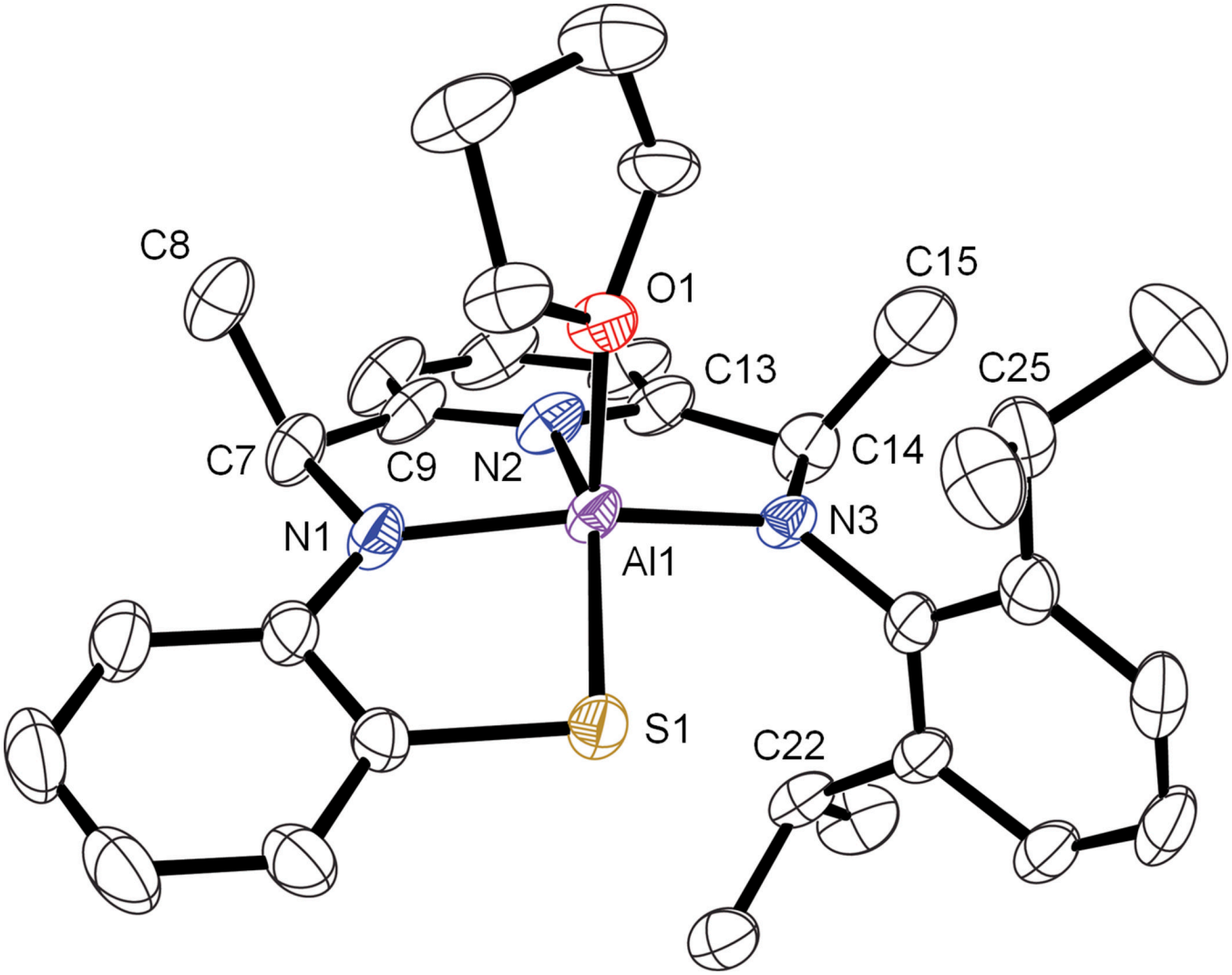

Figure 1.
Displacement ellipsoid plot (50% probability level) of diastereomer **2a**. H atoms and lattice solvent molecules are omitted for clarity.

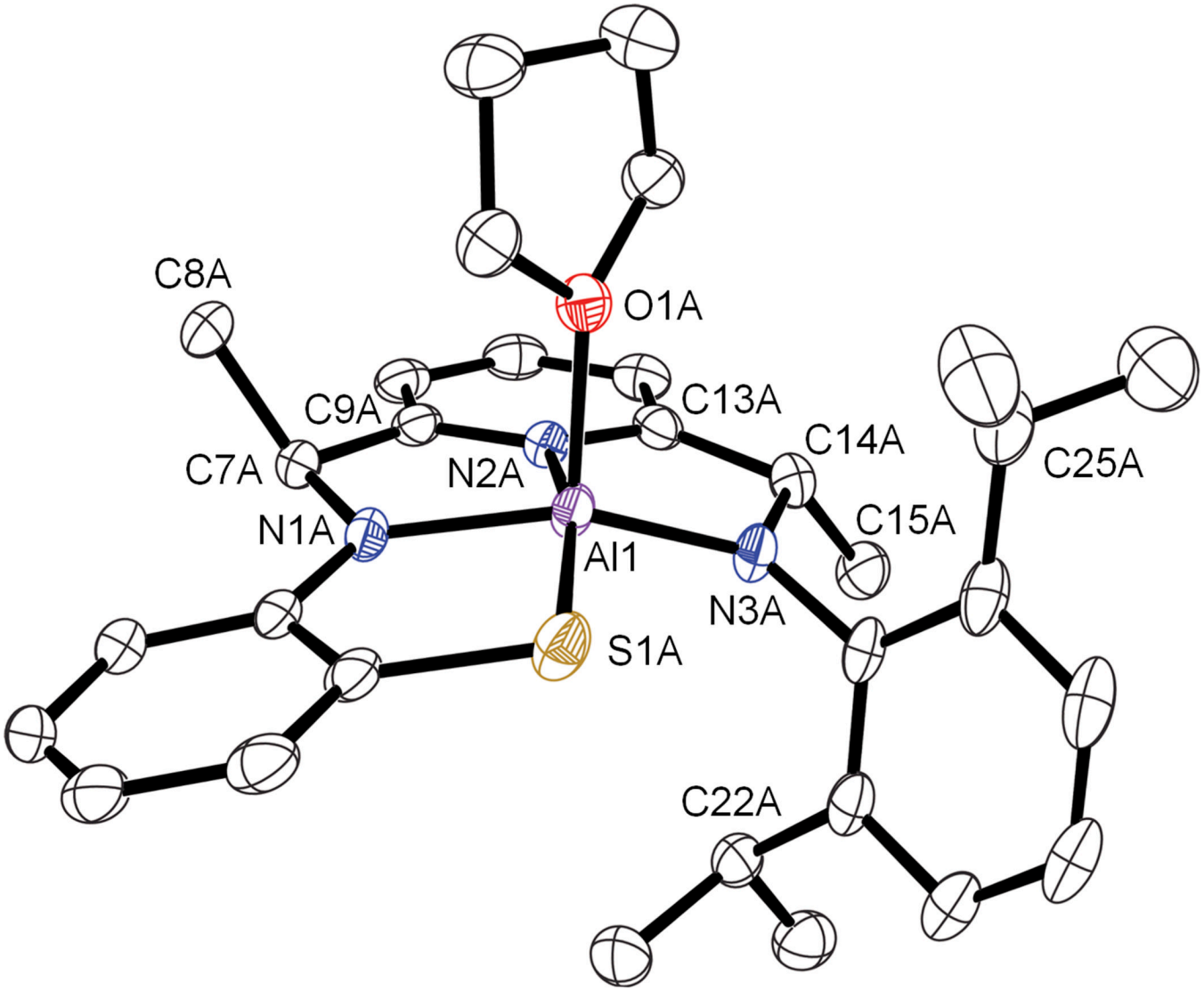

Figure 2.
Displacement ellipsoid plot (50% probability level) of diastereomer **2b**. H atoms and other crystallographically independent molecules are omitted for clarity.

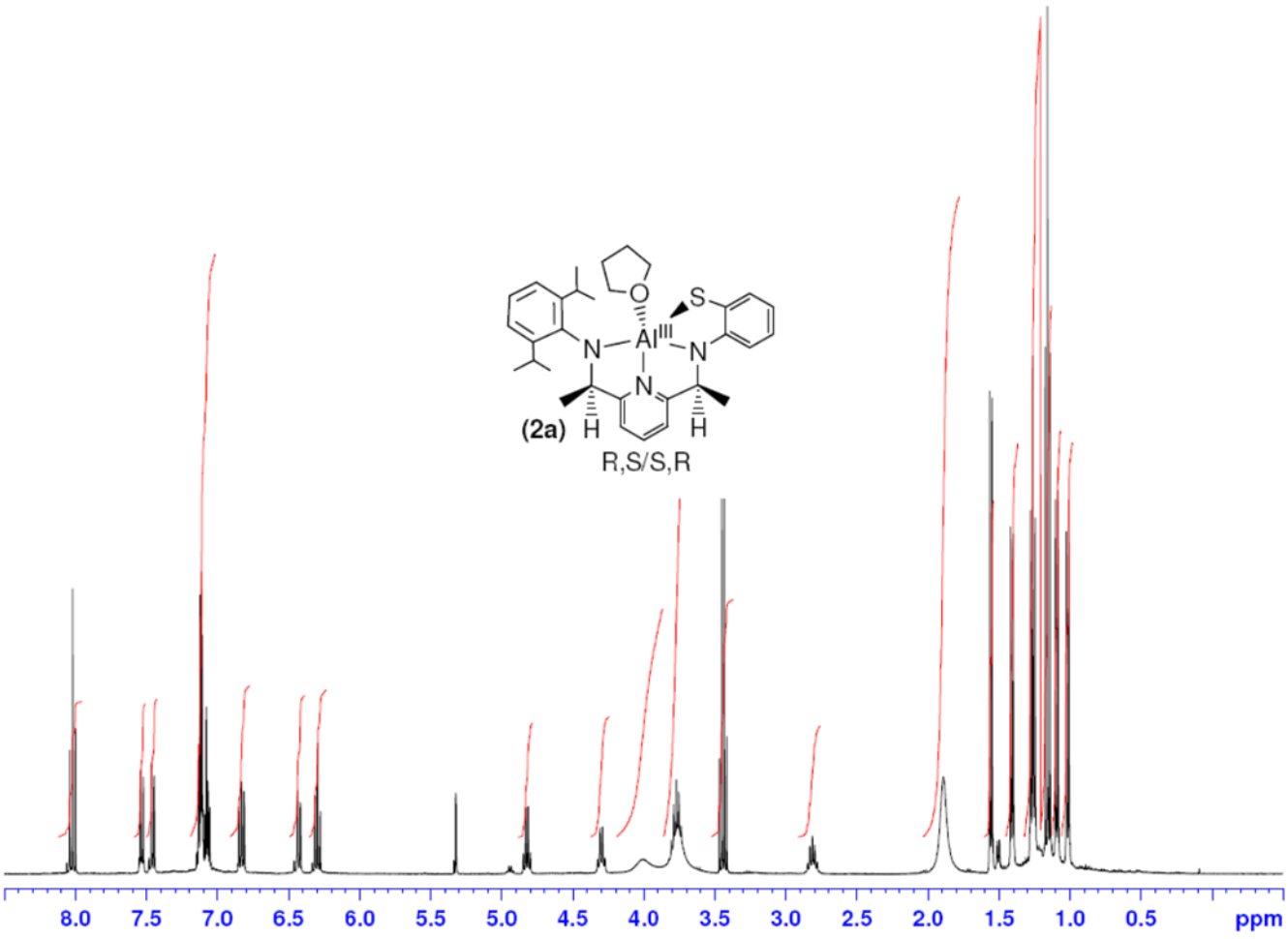

Figure 3.
^{1}H NMR spectrum of **2a**.

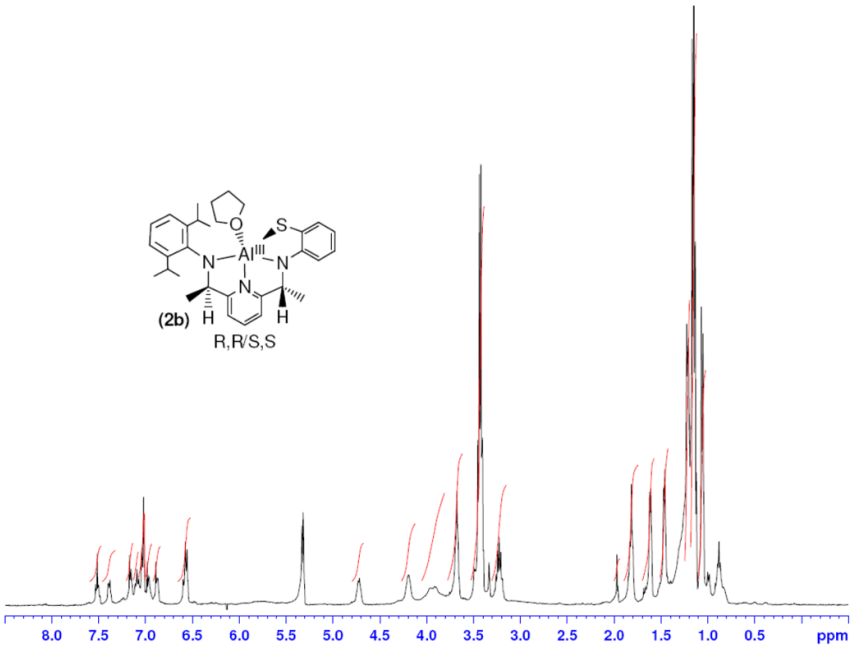

Figure 4.
^{1}H NMR spectrum of **2b**.

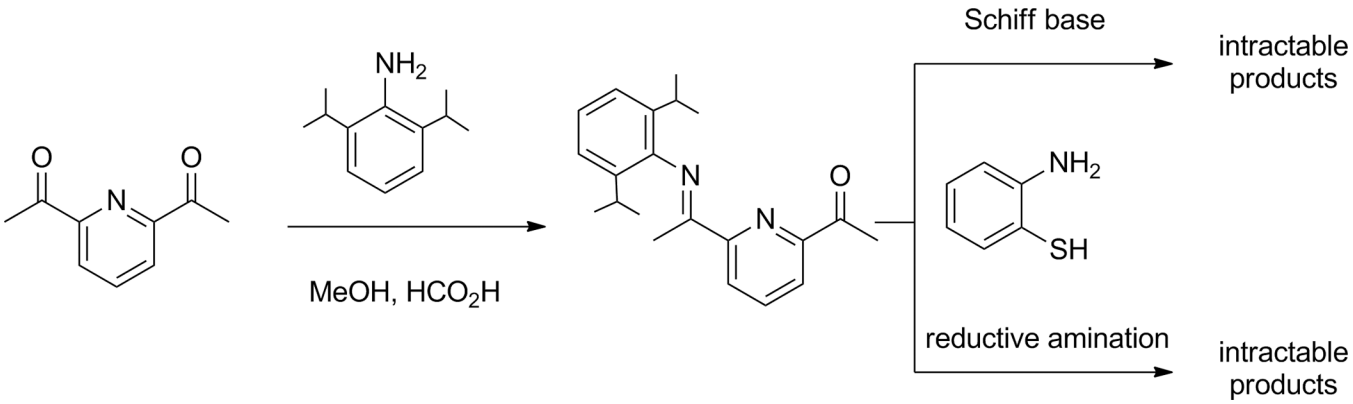

Scheme 1.

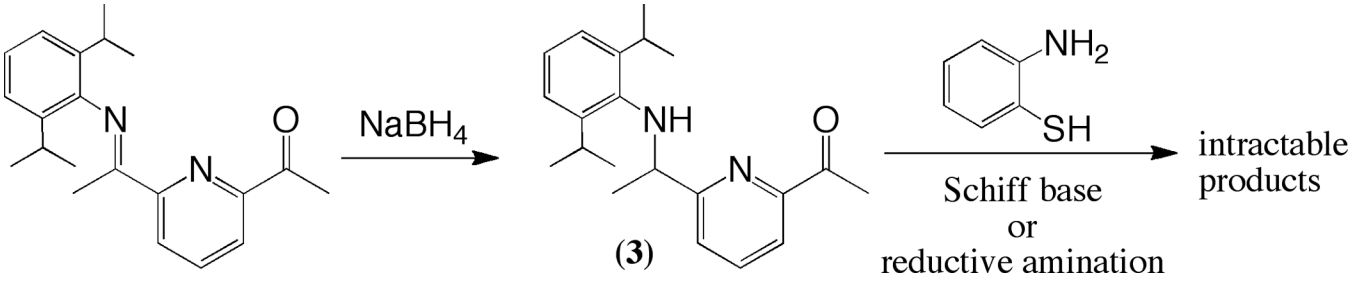

Scheme 2.
Synthesis of **3**.

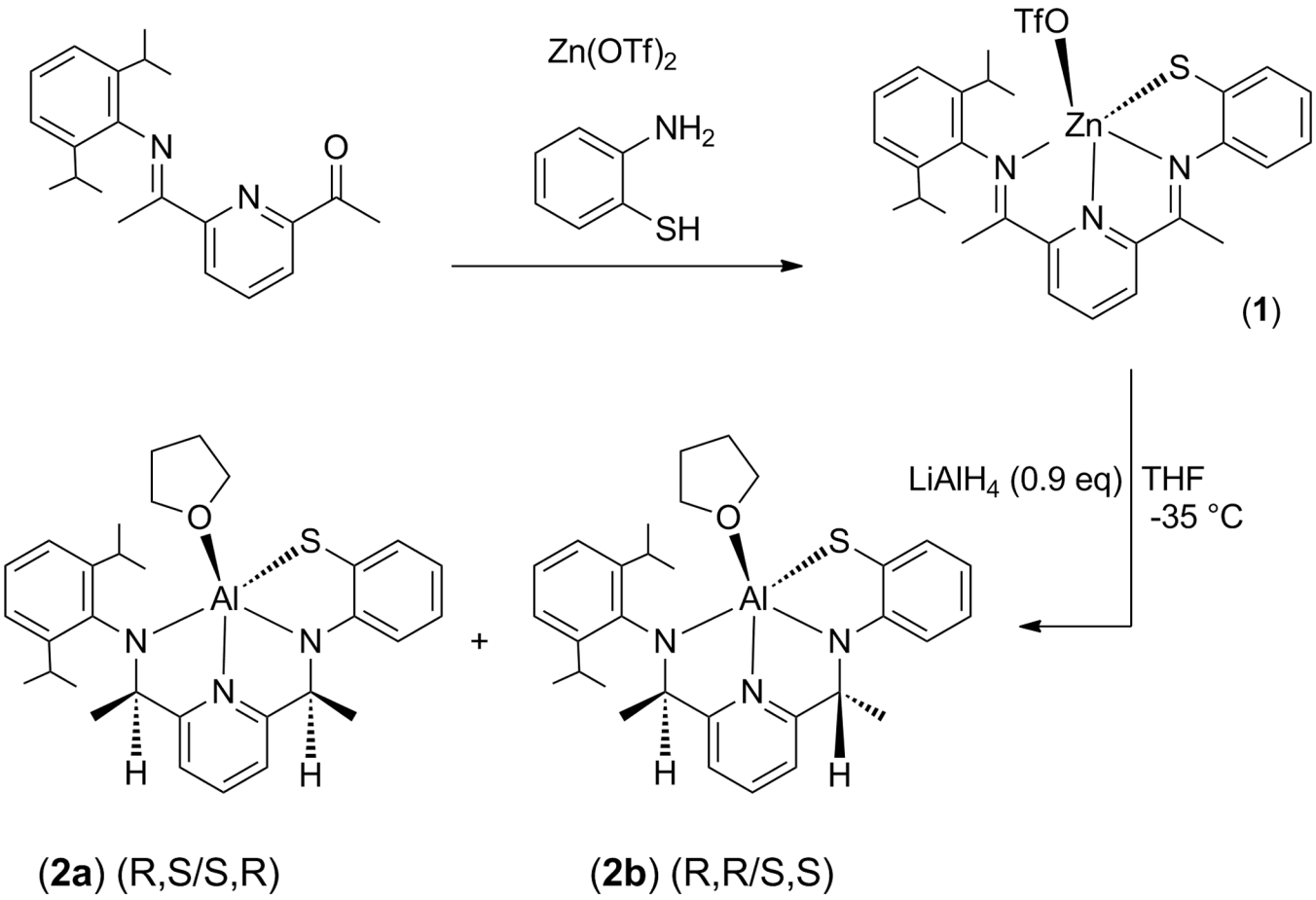

Scheme 3.
synthesis of the Al^{III} complexes **2a** and **2b**.

Table 1

Crystallographic data for complexes **2a–b**.

	(2a)	**(2b)**
Chemical formula	$2(C_{31}H_{40}AlN_3OS)\cdot C_4H_{10}O$	$C_{31}H_{40}AlN_3OS$
Formula weight	1133.52	529.70
Crystal system	Triclinic	Triclinic
Space group	*P*-1 (#2)	*P*-1 (#2)
a (Å)	8.8009 (2)	12.54209 (18)
b (Å)	13.7366 (4)	15.8805 (2)
c (Å)	13.9119 (5)	17.5832 (3)
α (°)	111.716 (3)	68.5229 (14)
β (°)	93.621 (2)	89.6375 (12)
γ (°)	91.141 (2)	73.0413 (13)
V (Å^3)	1557.69 (8)	3097.32 (8)
Z	1	4
μ (mm^{-1})	0.16	0.16
Crystal size (mm)	0.40 × 0.25 × 0.14	0.42 × 0.38 × 0.21
T_{min}, T_{max}	0.965, 0.985	0.948, 0.974
No. of measured, independent and observed [$I > 2\sigma(I)$] reflections	15662, 5478, 3770	54514, 12182, 9655
R_{int}	0.049	0.056
$R[F^2 > 2\sigma(F^2)]$, $wR(F^2)$, S	0.049, 0.136, 1.02	0.042, 0.124, 1.08
No. of reflections	5478	12182
No. of parameters	402	679
No. of restraints	43	0
H-atom treatment	H atoms treated by a mixture of independent and constrained refinement	H-atom parameters constrained
$\Delta\rho_{max}$, $\Delta\rho_{min}$ (e Å^{-3})	0.32, −0.36	0.41, −0.47

Table 2

Selected bond lengths (Å) and angles (°) for **1**, **2a**, **2b** and [$Fe^{II}(LN_3S)OTf$].

	2a	**2b**[a]	**1**[b]	**$Fe^{II}(LN_3S)(OTf)$**
ref	This work	This work	26	26
M^e-N1	1.887(2)	1.8763(13)	2.202(2)	2.188(2)
M-N2	1.967(2)	1.9590(13)	2.049(2)	2.072(2)
M-N3	1.862(2)	1.8560(13)	2.173(2)	2.184(2)
M-S1	2.2798(9)	2.2796(6)	2.2521(8)	2.2942(8)
M-O1	1.9320(18)	1.9485(11)	2.0940(18)	2.0870(18)
N1-C7	1.462(3)	1.4559(19)	1.283(3)	1.293(3)
N3-C14	1.465(3)	1.4714(19)	1.278(3)	1.284(3)
N1-M-N2	79.93(9)	79.91(5)	74.54(9)	73.89(9)
N1-M-N3	154.19(10)	146.83(6)	148.80(8)	146.47(8)
N1-M-S1	87.18(7)	88.84(4)	85.33(6)	82.95(6)
N1-M-O1	97.93(9)	100.96(5)	97.56(8)	98.91(8)
N2-M-N3	81.33(9)	80.50(5)	75.51(9)	74.32(8)
N2-M-S1	153.69(8)	165.36(4)	143.22(7)	139.13(6)
N2-M-O1	100.03(8)	92.17(5)	99.75(8)	102.77(8)
N3-M-S1	102.34(7)	104.84(4)	114.62(6)	115.57(6)
N3-M-O1	102.69(8)	106.28(6)	95.88(8)	98.20(8)
S1-M-O1	104.43(6)	99.20(4)	113.38(6)	113.92(6)
N1-C7-C9	105.9(2)	106.30(12)	113.7(2)	113.9(2)
N3-C14-C13	107.7(2)	106.79(12)	115.7(2)	115.9(2)

[a] Data taken from only one of two distinct, but similar molecules in the asymmetric unit.

[b] Data taken from only one of three distinct, but similar molecules in the asymmetric unit.

[c] M equals Al1 in **2a** and **2b**, Zn1 in **1,** Fe1 in the [$Fe^{II}(LN_3S)(OTf)$].